Polymer Melts under Uniaxial Elongational Flow: Stress−Optical Behavior from Experiments and Nonequilibrium Molecular Dynamics Computer Simulations

M. Kröger,* C. Luap,† and R. Muller†

Institut für Theoretische Physik, Technische Universität Berlin, PN 7--1, Hardenbergstr. 36, D-10623 Berlin, Germany, and Institut Charles Sadron (CRM/EAHP), 4 rue Boussingault, F-67000 Strasbourg, France

Received February 27, 1996; Revised Manuscript Received June 29, 1996[⊗]

ABSTRACT: Tensile stress and birefringence in both real and model amorphous polymer melts have been measured during constant rate uniaxial elongational flow. We focus on investigations where deviations from the linear stress−optical behavior are pronounced. A rate-dependent contribution to the stress which is not directly related to the intramolecular conformations ("stress offset") is detected for both types of macromolecular fluids. Independent of the flow history, during relaxation a linear stress−optical behavior is revealed. Nonequilibrium molecular dynamics (NEMD) computer simulations on the multibead anharmonic spring model are shown to provide insight into the molecular mechanisms underlying the viscoelastic behavior: during relaxation the intermolecular interactions become dominant in correlation with linear stress−optical behavior; the stress offset is shown to be very similar to the stress arising in the corresponding simple fluid; the total stress can well be approximated by a sum of three parts which are based on single-particle and single-link distribution functions only; the yield point behavior at high elongation rates reflects the transition from affine to nonaffine motion of bonds and is understood without reference to strong inhomogeneities resulting from local plastic strain production [the chemical structure does not influence the qualitative behavior]; distinct microscopic stress contributions under elongation and subsequent relaxation such as inter- and intramolecular, attractive and repulsive, kinetic and potential contributions are resolved.

I. Introduction

Molecular dynamics computer simulations provide a powerful tool to investigate the microscopic origins of experimentally observable transport phenomena. For monodisperse amorphous polymer melts, Kremer and Grest[1] have performed extensive equilibrium simulations to investigate the different regimes of the diffusive motion of a polymer chain. This approach has been extended to flow phenomena such as shear flow[2,3] and elongational flow for polymer melts,[4−6] polymer solutions,[7,8] and more recently, to living polymer systems.[9] Nonequilibrium molecular dynamics (NEMD) computer simulations provide a wealth of information about the interrelation between the peculiar rheology of polymer melts and the underlying microstructural changes, i.e., flow-induced alignment or stretching of segments, distortions of the diverse pair-correlation functions far from their equilibrium values[5,10] or the variations of entanglement densities.[11]

Simulations have to be based on simple models. Hence it is important to confirm their relevance by comparison with experimental data. This approach was successfully pursued for the case of concentrated colloidal suspensions[12−14] and for polymer melts under shear flow,[3,15] where scattering patterns from small-angle neutron scattering (SANS) and rheological data could be favorably compared with data obtained from NEMD simulations. Furthermore, the NEMD simulations allow for a test of some commonly used assumptions of the different theoretical models.

In this paper we report results for stress and birefringence in both real and model polymer melts as measured during constant rate uniaxial elongational flow which is followed by relaxation after reaching a given stretching ratio. We focus on system and flow parameters where deviations from the linear stress−optical behavior are pronounced, i.e. at temperatures close to the glass transition temperature (T_g) or high elongation rates.

The phenomenological description of the viscoelastic behavior of amorphous polymers in the glass transition region has been adjusted many times within the last decades.[4,16−21] Birefringence studies during stress relaxation, creep, or dynamic mechanical experiments motivated others to consider two coupled contributions to the molecular motions, one of these involving stresses of predominantly entropy−elastic origin (σ_{or}), the other involving energy−elastic stresses (σ_d).[19,20] A modified stress−optical rule (MSOR), $\Delta n(t) = C_d\sigma_d(t) + C_{or}\sigma_{or}(t) = C(t)\sigma(t)$, was proposed, where $\sigma \equiv \sigma_{or} + \sigma_d$ denotes any component of the deviatoric (anisotropic) stress tensor, Δn is the corresponding "uniaxial" component of the refractive index tensor, and C_{or}, C_d are material constants. This MSOR was tested experimentally on a large number of polymers.[21] During stress relaxation or creep, the birefringence/stress ratio $C(t)$ is not constant but typically increases with time. The indexing of the two contributions is motivated by the work of Priss et al.[19] and Read[20] due to a molecular picture which involves on one hand relatively long-range conformational rearrangements which are associated with the (dis)orientation (index *or*) of main-chain segments (entropic−elastic contribution) and on the other hand local energy−elastic displacements (index *d*), such as the torsion around main-chain bonds against rotational energy barriers and the increase and decrease in interchain spacing[17] opposed by the forces of attraction and repulsion. The orientational stress then dominates the stress arising in polymers far away from the glass transition temperature (T_g) where the usual stress−optical rule (SOR), i.e. the MSOR with $C_d = 0$, is mostly

* Corresponding author. E-mail: mk@polly.physik.tu-berlin.de.
† Institut Charles Sadron.
⊗ Abstract published in *Advance ACS Abstracts,* December 15, 1996.

S0024-9297(96)00317-8 CCC: $14.00

valid.[16,18] In expressing the stress tensor as a function of the local stress components defined in a frame fixed to the molecules backbone and writing these components as a sum of a constant and fluctuations, Gao and Weiner[4] derived an expression for the stress which includes a term proportional to the orientation of the molecule's backbone and an additional term due to the fluctuation of the local stress in the molecular frame. In taking the constant they were motivated by their molecular dynamics simulation studies of a polyethylene-like polymer model.[4,22] In ref 4 the distortional stress was related to the stress arising from a displacement of all mers that corresponds to the macroscopic affine deformation at short times. Even for simple fluids the affine stress mechanism occurs, but on a much smaller time scale than for macromolecular liquids since the atoms are not constrained by covalent bonds.

The aim of the present paper is to get insight into the molecular sources of nonlinear viscoelasticity for polymer melts and to compare with phenomenological pictures as well as to clarify their relevance for the interpretation of results on both model polymers and real polymers under elongation/relaxation. While from experiments the macroscopic stress and refractive index tensors are determined, from the simulations on a model system made of beads, the distinct contributions to the stress and alignment of segments are calculated from the bead trajectories. In turn it allows localization of the microscopic origin of stresses arising in the model polymer melt. The simulation technique as used here neglects chemical details and suppresses any macroscopic density fluctuations which do occur in real systems. But the strong qualitative similarities between the available experimental information and the results of the model fluids motivate us to clarify some points on the molecular origins of nonlinear viscoelasticity.

This article is organized as follows: The experimental conditions and results are presented in section II. Birefringence data and stress−optical diagrams are given for samples at different temperatures/elongation rates. The deviations from the linear SOR are analyzed. The molecular model for the simulated polymer melt is described in section III. The microscopic expressions for specific contributions to the macroscopic stress as well as for the segment alignment (birefringence) are given in section IV. Quantities are defined which measure the anisotropy and inhomogeneities at different intramolecular length scales. In section V the simulation results are presented. They are discussed and compared with the experimental results in section VI.

II. Experimental Results

In continuation of previous experiments,[16] we study in detail the rate dependence of the stress−optical behavior of amorphous polymers undergoing elongational flow at temperatures just above the glass transition temperature (T_g). Experiments reported here have been carried out on a commercial polystyrene from Elf-Atochem (Lacqrène 1241 H). Its glass transition temperature, as determined by differential scanning calorimetry at a heating rate of 10 °C/min, is 95 °C. The investigated polystyrene has a molecular weight of M_w = 330 000 with a polydispersity of M_w/M_n = 2.5. Its zero shear viscosity at 173 °C is $\eta_0 = 1.6 \times 10^5$ Pa s. Simultaneous measurements of stress and birefringence have been performed by using an extensional rheometer[25] during deformation at constant elongation rate. The stress−optical behavior accompanying the relaxation at constant values of deformation and temperature was studied as well.

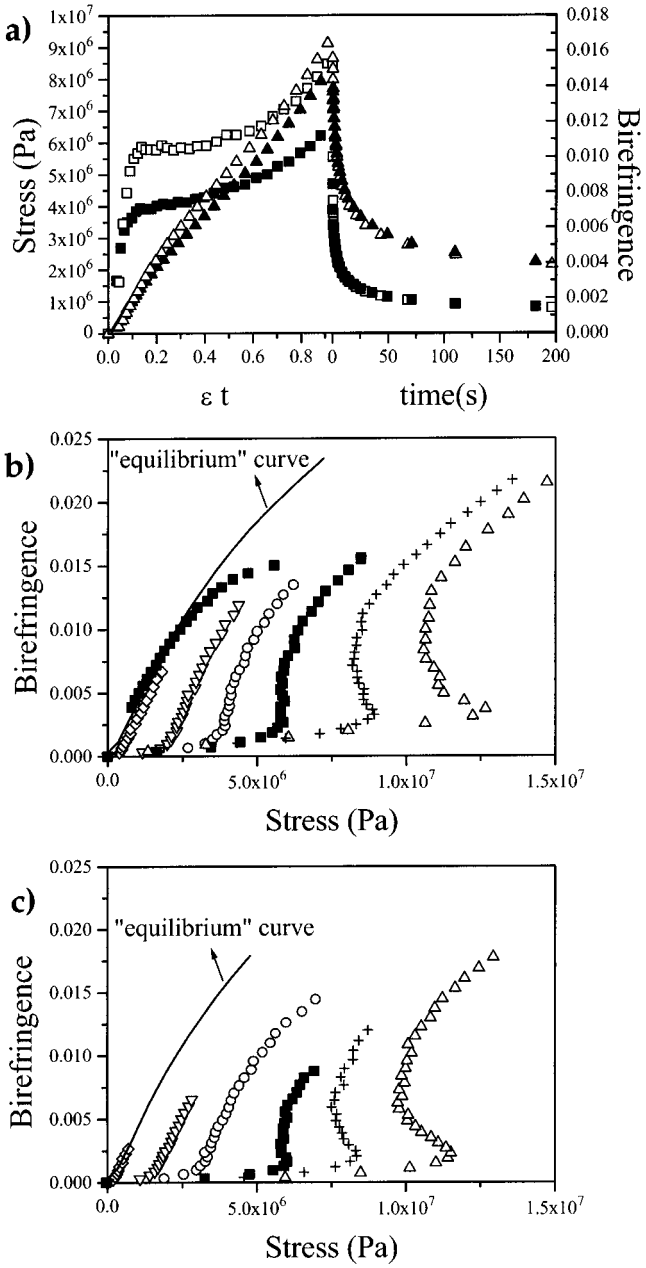

Figure 1. Experimental data. (a) Tensile stress (□) and birefringence (△) vs dimensionless time ($t\dot{\epsilon}$) for two elongation rates and subsequent relaxation at T = 102.7 °C, $\dot{\epsilon} = 0.1$ s^{-1} (filled symbols) and $\dot{\epsilon} = 0.2$ s^{-1} (open symbols). (b) Birefringence vs tensile stress at temperature T = 102.7 °C. Elongation rates: 0.01 (◇); 0.05 (▽); 0.1 (○); 0.2 (■); 0.5 (+) and 1 s^{-1} (△). For one rate ($\dot{\epsilon} = 0.2$ s^{-1}) a relaxation curve after the macroscopic flow is stopped is included. (c) Birefringence vs tensile stress at temperature T = 97.9 °C. Elongation rates: 5×10^{-4} (◇); 5×10^{-3} (▽); 0.01 (○); 0.03 (■); 0.05 (+) and 0.1 s^{-1} (△).

Stress−Optical Behavior at Various Elongation Rates. The curves in Figure 1a show a typical example of the time variation of both true tensile stress and birefringence during elongation and relaxation for two different rates at temperature T = 102.7 °C. From such sets of curves, the stress−optical diagrams, i.e., birefringence versus true stress as obtained at various elongation rates for T = 102.7 and 97.9 °C, are plotted in Figure 1, parts b and c, respectively. These data

clearly show departure from the linear SOR. The "equilibrium curve" as defined by Pesce and Muller is taken from ref 16.

The typical behavior can be described as follows: the fast stress growth at the early stage of the deformation induces only a weak increase of the orientation; when the stress has reached a finite value, the birefringence starts to increase with stress in a way similar to the high temperature behavior. As soon as the flow is stopped, the stress relaxes rapidly and the "equilibrium curve" is recovered (Figure 1b; $\dot{\epsilon} = 0.1\ s^{-1}$).

Temperature and Rate Dependence of the Stress Offset. The deviations from the classical SOR can be described by an additional stress contribution[16] which arises when the temperature becomes close to T_g. This contribution, which is not related to the flow-induced orientation, is nearly constant for a given elongation rate and appears as a "stress offset" in the stress−optical diagram. The relaxation behavior along the "equilibrium curve" indicates that its relaxation is fast in comparison with the orientation relaxation.

Figures 1b,c show that the stress offset depends strongly on the rate. It becomes important with increasing elongation rate at a fixed temperature or with decreasing temperature at fixed rate. For the lowest rates (5×10^{-4} and $0.01\ s^{-1}$ for 97.9 and 102.7 °C, respectively), only small deviations from the "equilibrium curve" can be detected. For the highest rates, the curves show the stress overshoot (we will call it "yield point") typically observed for glassy polymers undergoing plastic deformation.

Application of Time-Temperature Superposition Principle. In Figure 2a we have reported approximate values of the stress offsets versus the reduced elongation rate $a_T\dot{\epsilon}$ as obtained from Figure 1b,c, the reference temperature being 97.9 °C. This figure has been obtained by plotting, on double logarithmic scale, the stress offset versus elongation rate for both temperatures and then data at 102.7 °C have been shifted horizontally by a factor of $\log a_{T=102.7\rightarrow 97.9°C} = -0.98$ (Figure 2b). In the range of low elongation rate ($a_T\dot{\epsilon}$ s^{-1}), a linear dependence of the stress offset on rate is found. The onset of the departure from linearity corresponds to the reduced elongational rate for which a stress overshoot (yield point) in the stress−strain curve appears. At high rates the stress offset seems to reach an asymptotical value [In this regime, the stress offset is measured in the time (or birefringence) range for which a nearly constant departure from the equilibrium curve can be defined]; Data for reduced elongational rates higher than those reported here were not available because of a systematic failure of specimens.

It should be mentioned that the shift factor used to superpose the curves of Figure 2b is in agreement with the value deduced from dynamic shear moduli measurements within a large temperature range. For reasons of completeness, experimental shift factors versus temperature, for a reference temperature of 173 °C, are plotted in Figure 2c. An extrapolation of experimental log a_T values in the low temperature range (dotted line) gives $\log a_{T=102.7\rightarrow 97.9°C} \simeq -1.07$. The time temperature superposition principle for uniaxial elongational flow is

$$\sigma(t,\dot{\epsilon}_0,T_0) = \sigma\left(a_{T\rightarrow T_0}t, \frac{\dot{\epsilon}_0}{a_{T\rightarrow T_0}}, T\right)$$

$$\text{with} \quad a_{T\rightarrow T_0} = \frac{\eta_0(T)}{\eta_0(T_0)} \quad (1)$$

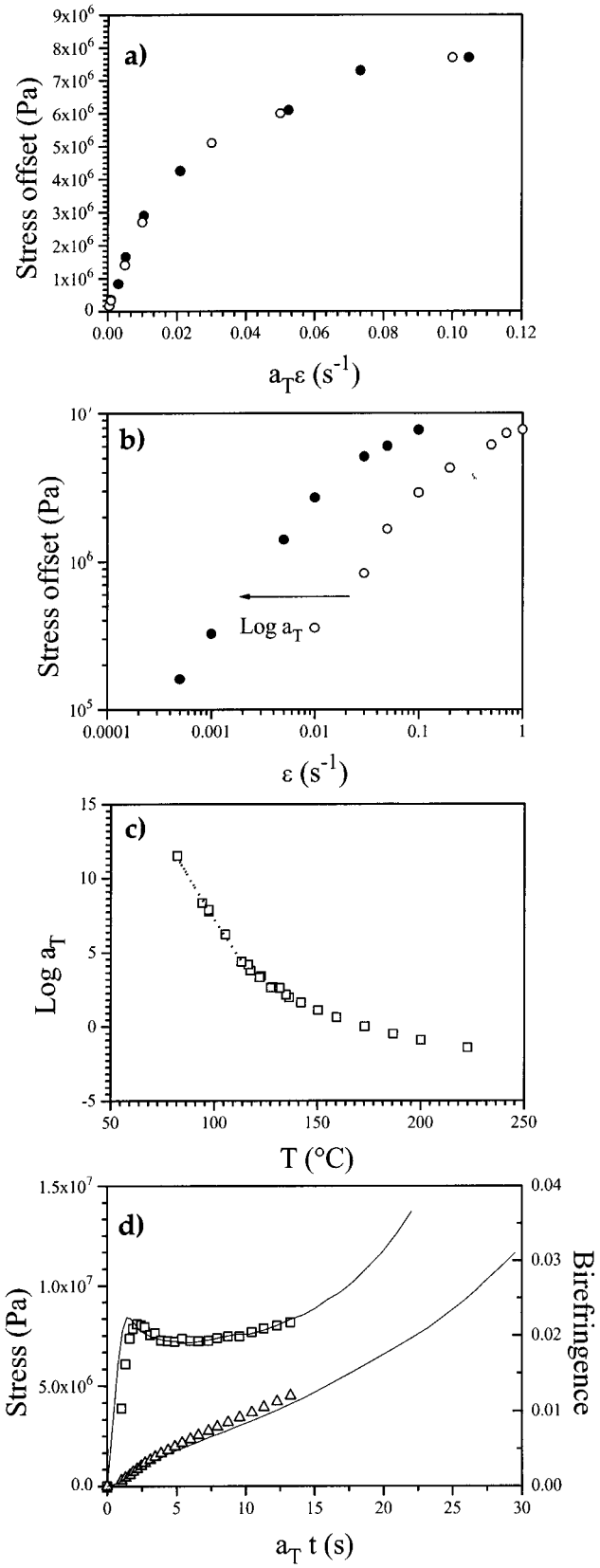

Figure 2. Experimental data. Stress offset vs (a) the reduced elongation rate $\dot{\epsilon}a_T$ and (b) the elongation rate for two temperatures ($T = 102.7$ °C and 97.9 °C (filled symbols)). The reference temperature in a) is 97.9 °C. (c) "Time−temperature superposition shift factor" log a_T vs temperature as determined by measurement of the frequency dependent dynamic shear moduli. The reference temperature is 173 °C. (d) Tensile stress (□) and birefringence (△) vs the reduced time $a_T t$ for $T = 97.6$ °C (reference temperature), $\dot{\epsilon} = 0.05\ s^{-1}$ and for $T = 94.6$ °C, $\dot{\epsilon} = 0.01\ s^{-1}$ (full line).

with $\eta_0(T)$ being the zero-shear viscosity at temperature T. To test its applicability for stress optical behavior near the glass transition temperature as suggested by above presented results, we have compared experiments performed at two different temperatures and rates: $T_0 = 97.6$ °C with $\dot{\epsilon}_0 = 0.05$ s^{-1} and $T_1 = 94.6$ °C with $\dot{\epsilon}_1 = 0.01$ s^{-1}. The ratio between the two elongation rates corresponds to the value $a_{T_1 \to T_0}$, as determined from the data of Figure 2c (log $a_{T=94.6 \to 97.6°C} \simeq +0.7$). The measured birefringence and stress are plotted in Figure 2d versus the reduced time $a_T t$, the reference temperature being 97.6 °C. In view of the strong temperature and rate dependence of mechanical properties and the low accuracy of a_T data in the glass transition range, a surprisingly good correspondence between these curves can be observed. However, further experiments are needed to conclude on the thermorheological simplicity for the stress−optical behavior near T_g in view of the failure of the thermorheological simplicity reported earlier from dynamic rheooptical analysis of polystyrene.[26]

Remarks on Experimental Findings. Analysis of our data with the MSOR[20,26] would lead to a distortional or glassy stress comparable to the stress offset, as the stress−optical coefficient at the glassy state is more than 100 times lower than at the rubbery state (for polystyrene, $C_d \simeq 10^{-11}$ Pa^{-1} and $C_{or} \simeq -5 \times 10^{-9}$ Pa^{-1}, respectively).[26] For all experiments reported here, birefringence values are always negative (plotted in absolute value); the distortional contribution to birefringence (which would give a positive contribution) is thus absent or small in comparison to the orientational contribution within the studied temperature/rate range. Results of polystyrene very similar to these have been also found via infrared dichroism.[27] Moreover, in a recent study of polycarbonate,[28] simultaneous measurements of stress and infrared dichroism for several absorption bands have shown that both techniques lead to the same qualitative behavior independent of the considered functional groups (main or side chain).

Hence the phenomenon analyzed here should be independent of the detailed chemical structure of chains and regarded as a failure of proportionality between the stress and the second moment of the orientation distribution function of the chains backbone. Both quantities can be independently analyzed from computer simulations on model polymer melts as will be described next.

III. The Microscopic FENE Chain Model

Recent results have shown that simulations can be used to predict rheological behavior of real polymer melts, even if the simulation model does not contain specific chemical details[3,4,29,30] in accordance with predictions on self-similarity and universality in polymer systems.[31] To study the elongational flow behavior of model polymer melts, we have performed NEMD computer simulations at constant bead density and constant volume (NVT ensemble) in a cubic cell with periodic boundary conditions. Each linear chain consists of N beads connected by an anharmonic FENE spring.[1,5,32]

All the beads interact with a repulsive Lennard−Jones (LJ) potential[33]

$$U_{ij}^{LJ} = 4[(r_{ij}^*)^{-12} - (r_{ij}^*)^{-6} + 1/4] \quad \text{for} \quad r_{ij}^* \le 2^{1/6} \quad \text{and}$$

$$U_{ij}^{LJ} = 0 \text{ for } r_{ij}^* \ge 2^{1/6} \qquad (2)$$

where r_{ij}^* is the distance between bead i and j (1, ..., N).

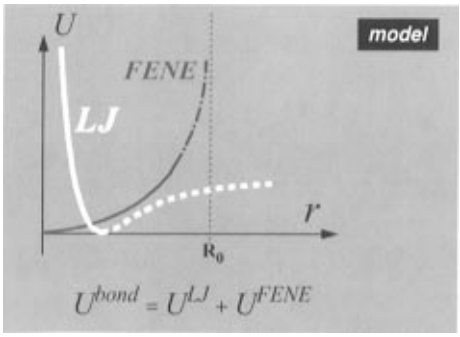

Figure 3. The potentials specifying the microscopic model which is studied by NEMD computer simulations.

Here and in the following all quantities which are reduced to the usual LJ units are denoted by an asterisk if ambiguities could otherwise arise. For beads which are nearest neighbors along the chain (for $N > 1$), an attractive potential (FENE potential) is added (Figure 3):

$$U_{ij}^{FENE} = -0.5k^*R_0^2 \ln[1 - (r_{ij}^*/R_0)^2] \quad \text{for} \quad r_{ij}^* \le R_0 \quad \text{and}$$

$$U_{ij}^{FENE} = \equiv \quad \text{for} \quad r_{ij}^* \ge R_0. \qquad (3)$$

With the choice for the finite extensibility of the FENE spring $R_0 = 1.5$ and $k^* = 30$, we follow previous investigations.[1,3,5,10] Newton's equations of motion for the three-dimensional model system are solved using the velocity Verlet algorithm.[34] Neighbor lists and the layered link cell algorithm,[35] Lees−Edwards boundary conditions,[36] a velocity rescaling temperature control mechanism,[29] and the homogeneous shear algorithm of Evans[37] modified for isochoric elongational flows[5] were used to produce the simulation results for bulk properties. Details of the implementation of the efficient algorithm can be found elsewhere.[1,5,35] In the computer experiments, the transient fluid behavior is obtained by averaging nonequilibrium trajectories in logarithmically equidistant time steps over 30 initial equilibrium configurations for every choice of parameters.

In the next section definitions are given for which NEMD results will be presented in section V.

IV. Microscopic Expressions for Extracted Quantities

Stress Tensor. The stress tensor $\sigma_{\mu\nu}$ (by adding the kinetic and potential contribution) is calculated from its microscopic definition

$$\sigma_{\mu\nu} = -\frac{1}{V}\left(\sum_{i=1}^{N_b} v_{\mu i} v_{\nu i} - \frac{1}{2}\sum_{i=1}^{N_b}\sum_{j=1}^{N_b} \frac{r_{\mu ij} r_{\nu ij}}{|r_{ij}|} \frac{dU_{ij}}{dr_{ij}}\right) \qquad (4)$$

where V is the volume of the simulation cell, N_b is the total number of beads, v_{xi} is the x component of the (peculiar) velocity v of bead i within a polymer chain, r_{xij} is the x component of r_{ij}, and U_{ij} is the pair potential (here $U = U^{LJ} + U^{FENE}$). A time-dependent uniaxial isochoric homogeneous elongational flow in the x-direction with elongation rate $\dot{\epsilon} = \partial v_x/\partial x$ is imposed. At fixed deformation the relaxation behavior toward the equilibrium state is investigated. Rheological information under uniaxial flow is contained in the "uniaxial" component of the stress tensor or "tensile stress": $\sigma \equiv \sigma_{xx} - (\sigma_{yy} + \sigma_{zz})/2$.

Flow Alignment of Polymer Segments. The (second rank) segment alignment tensor, the anisotropic second moment of the orientation distribution function of a specific segment i on the chains backbone,[5,38]

$$\mathbf{a}(i) \equiv \langle \mathbf{u}_i \mathbf{u}_i \rangle - \frac{1}{3}\mathbf{I} \quad \text{with} \quad i = 1, ..., N-1 \qquad (5)$$

is extracted directly as an ensemble average from the dyadic constructed of the normalized segment vectors $\hat{\mathbf{u}}_i = \mathbf{u}_i/u_i$ (with $u_i = |\mathbf{u}_i|$) within the polymer chains, each linear chain being made of N connected beads. The alignment tensor $\mathbf{a} = \sum_i^{N-1} \mathbf{a}(i)/(N-1)$ is anisotropic and proportional to the refractive index tensor of the fluid[18] for which the relevant information for the case of uniaxial elongational flow in the x-direction we denote by $\Delta n \equiv a_{xx} - (a_{yy} + a_{zz})/2$. It is experimentally accessible by measuring the orientational birefringence (section II). Correspondingly the distribution of segment lengths, the square of radius of gyration $R_g^2 \equiv \sum_{i>j}^{N} \sum_{k,l=j}^{i-1} \langle \mathbf{u}_k \cdot \mathbf{u}_l \rangle / N^2$ or the end-to-end distance of polymers R_e are calculated from the microscopic knowledge of all bead positions at any time step.

Contributions to the Stress Tensor. The interactions within the model polymer melt can be divided into classes with respect to their distinct molecular origins. During the simulations, the following contributions, with different physical nature, to the microscopic expression of the potential part σ_{pot} of the stress tensor are extracted stemming from: attractive/repulsive interactions between nearest neighbors within chains (σ_{nn}^{att}, σ_{nn}^{rep}), interactions between *non*-nearest neighbors within chains (σ_{nnn}), intermolecular interactions between beads of different chains (σ_{int}), and kinetic contribution of all beads to the total stress (σ_{kin}). The quantity $\sigma_{off} \equiv \sigma_{pot} - \sigma_{nn} - C^{-1}\Delta n$ will be used to measure the "effective" stress offset, where C is the linear stress−optical coefficient as measured independently from both NEMD simulations on weak shear flows[3] and relaxation at constant stretching ratio (section V). In both cases we get the same value for C within 5% of accuracy.

Since at the beginning of our investigation our hypothesis was that the σ_{nn} mainly obeys a stress optic rule (SOR), the detected deviations (see sections II and V) especially at short times should originate from σ_{nnn} or σ_{int} or from collective stretching/contraction of neighboring bonds which would not necessarily influence the flow birefringence. Recently the Doi−Edwards model[23] has been extended to incorporate the effect of segmental stretch[24] into the equations, where all rheological properties are assumed to be dominated by intramolecular forces. The fast relaxation of the additional stress (offset) σ_{off} after reaching a constant stretching ratio (see section V) tends to show that it is related to local interactions and it is too fast to relax spatial inhomogeneities on a larger scale which in turn were one of the candidates made responsible for the yield point behavior.[39] Hence when constructing a molecular picture for the full process, the problem reduces to finding the microscopic origin of the stress offset, which motivated us to investigate all distinct contributions to the stress separately as well as to resolve quantities which measure collective deformations and local anisotropies.

Deformation and Orientation of Polymer Chains. To analyze the degree of stretching and orientation of the polymer chains on different length scales or

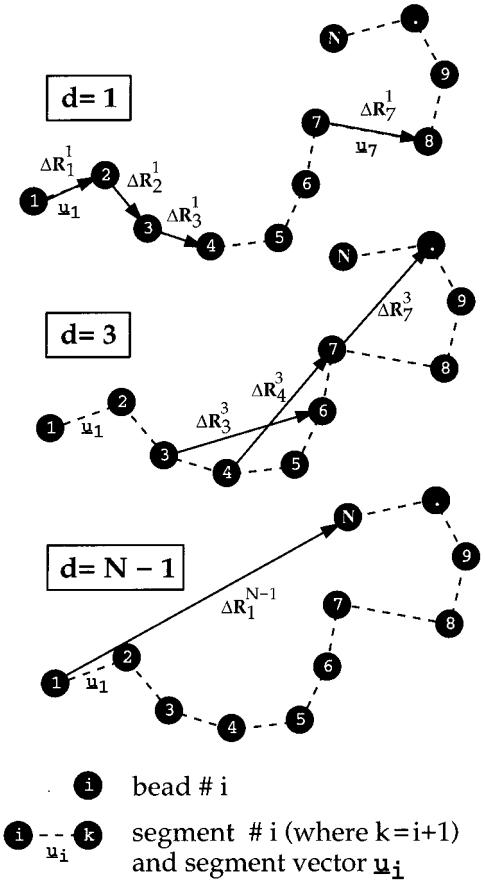

Figure 4. Schematic drawing of quantities arising in the definition of $\mathbf{F}(d)$ in eq 6 for three values for the contour distance d.

distances (measured along the chains backbone, now called "contour distance"), we introduce a tensor $\mathbf{F}(d)$ which characterizes a single chain on a contour distance $d \in 0, ..., N-2$ (a chain has $N-1$ segments).

$$\mathbf{F}(d) \equiv \frac{1}{N-d-1} \sum_{i=1}^{N-d-1} \Delta^d \mathbf{R}_i \Delta^d \mathbf{R}_i \quad \text{with} \quad \Delta^d \mathbf{R}_i = \sum_{j=i}^{i+d} \mathbf{u}_j \qquad (6)$$

where $\Delta^d \boldsymbol{R}_i$ is the vector pointing from bead i to bead $i + d$ of the chain (see Figure 4). The quantity $\langle \mathbf{F}(d) \rangle$ then denotes an average over all chains for an ensemble of systems. The "uniaxial" component of $\mathbf{F}$ is a measure for the alignment on different lengths scales d along the chains backbone. For this expression (which vanishes for an isotropic sample, i.e. at equilibrium here) as well as for the trace of $\langle \mathbf{F} \rangle$, there are bounds for each choice of d like for the birefringence value Δn, e.g., one has $\Delta n \in [-1,1]$.

To analyze the intramolecular localizability of neighboring stretching/contraction of bonds, we analyze the separate contributions to a discrete bond lengths autocorrelation function $G(d)$ with $d = 0, ..., N-2$ being again the segment distance along the chains contour:

$$G(d) \equiv \frac{1}{N-d-1} \sum_{i=1}^{N-d-1} (u_i - \bar{u})(u_{i+d} - \bar{u}) \quad \text{with} \quad \bar{u} = \frac{1}{N-1} \sum_{j=1}^{N-1} u_j \qquad (7)$$

Table 1. NEMD Parameters[a]

$\dot{\epsilon}$	Δt	total steps/1000	% elongation
0.001	5×10^{-3}	248.6	731
0.002	5×10^{-3}	203.9	768
0.005	5×10^{-3}	959.4	1122
0.01	4×10^{-3}	503.3	748
0.02	3×10^{-3}	203.9	340
0.05	2×10^{-3}	203.9	768
0.1	7×10^{-4}	159.1	304
0.2	5×10^{-4}	9.6	260
0.5	5×10^{-5}	78.6	219

[a] The maximum value for integration time steps needed to perform elongation runs without artificial chain breaks for the studied elongation rates is given. Also the total number of time steps and the corresponding final stretching ratio is given. Macroscopic quantities were averaged at logarithmically equidistant time steps.

which measures for every polymer chain the deviation of bond lengths from their mean value. The procedure is similar to the measurement of the orientational correlation distance (persistence length), which would involve the scalar products $\hat{\mathbf{u}}_i \cdot \hat{\mathbf{u}}_{i+d}$ instead of $(u_i - \bar{u})$-$(\bar{u}_{i+d} - \bar{u})$ in ref 7. An increase in the quantity $\langle G(d) \rangle$ is also a measure for the occurrence of intramolecular inhomogeneities in deviations from the equilibrium distribution of bond lengths. To distinguish between neighboring bond stretching and neighboring bond contraction, which lead to contributions with equal sign in ref 7, it is necessary to evaluate the contributions to $G(d)$ dependent on the signs of both operands separately. Therefore, we have $G = G_{++} + G_{--} + G_{\pm}$, where for example G_{++} is the part of G which is made up of pairs of stretched bonds only, i.e. for $u_i > \bar{u}$ and $u_{i+d} > \bar{u}$.

In view of the traditional picture which relates the validity of the SOR to the stress arising from nearest neighbors (σ_{nn}), it is clear that a deviation from the SOR would be expected from a change in the distribution of bond lengths $f(u)$ compared with the equilibrium state. On the basis of the knowledge of all particle positions, $f(u)$ is extracted. For the nonequilibrium situations studied here, all the quantities $\mathbf{F}(d)$,$G(d)$, and $f(u)$ are time-dependent.

V. Computer Simulations Results and Discussion

All simulation runs were performed at temperature $T^* = 1$ and bead number density $n^* = 0.84$.[3] Data will be presented for monodisperse polymer melts of $N_b = 8400$ beads arranged in FENE chains with $N = 30$ beads, respectively as well as for the corresponding simple fluid ($N = 1$). The chains are small enough to compute all quantities on a CRAY Y-MP4E/464 within some hours per run and large enough to obtain results which can be compared well with our experimental findings on high-molecular polymers, even if the crossover in zero rate shear viscosity from low to high molecular weight model polymer melts was found for chains with lengths $N \approx 100$.[10] The dependence of all quantities on the chain length (degree of polymerization) is not shown here in detail. Recent Brownian dynamics studies on the FENE chain model for dilute polymer solutions with different chain lengths are available.[2,7] The minimum time steps needed during the simulation runs to prevent chain breaks at different elongation rates are collected in Table 1. Our data for $N = 2$ (dimers) is also available and will be discussed verbally. Motivated by the validity of the time-temperature superposition relation (eq 1) instead of varying the temperature, the elongation rate has been chosen as the significant parameter.

Contributions to the Stress Tensor. In most theoretical approaches to the rheology of polymers, the intramolecular stress plays an important role in view of the validity of SOR, which connects the measured stress with an intramolecular quantity. In many cases the intramolecular stress is predicted to be proportional to the alignment tensor as is exactly the case for the Rouse model (for infinitely dilute polymer solutions), but not true for the FENE model. Gao and Weiner found out from their molecular dynamics studies that the covalent structure, which is oriented by deformation, causes a directional screening of the noncovalent interaction.[22] As a result, the noncovalent potential makes an increasing contribution to the deviatoric stress.

NEMD data for the total stress and its contributions arising at different initial elongation rates are shown in Figure 5 (elongation) and Figure 6 (subsequent relaxation) for both the polymer melts (a−e) and the simple fluid (f).

For two rates some of these data has been collected in Tables 2 and 3. The total stress in Figures 5a and 6a can be qualitatively well compared with the experimental results. With increasing rate, the length of the time interval of affine motion increases. This affine motion causes the strong stress increase at short times as we checked by computing the "affine stress" by setting $T = 0$ while calculating the bead trajectories starting from an equilibrium configuration. At high rates ($\dot{\epsilon} \geq 0.05$), a yield point (a stress overshoot) is pronounced in contrast to the behavior at the lowest rates ($\dot{\epsilon} < 0.05$), for which the SOR is approximatively valid. The characteristic relaxation time (t_R) of chains with $N = 30$ beads is $t_R \approx 150$.[1,3] It is one reason for the long time tail of σ_{nnn} (see Figure 6 or Tables 2 and 3), the long time behavior of which is out of the scope of this paper (see, e.g. ref 6).

Flow Alignment on Different Length Scales. The flow-induced alignment is measured via the components of the gyration tensor and the alignment tensor as outlined in section IV. NEMD data for these quantities are shown in Figure 7. The quantity ΔR_G is directly connected with the shape of the static structure factor at small wave numbers (Guinier regime), the quantity Δn is proportional to the double refractive index.[18]

In section IV we have defined the tensor $\mathbf{F}(d)$, which is a natural extension of measuring alignment of polymer molecules on different length scales d. The uniaxial component $\Delta n(d) \equiv \langle F_{xx} - (F_{yy} + F_{zz})/2 \rangle$ of $\langle \mathbf{F}(d) \rangle$ as defined in eq 6 is shown in Figure 8b.

Notice that for $d = 0$: $\mathbf{F}(0) = \sum_{i=1}^{N-1} \mathbf{u}_i \mathbf{u}_i/(N-1)$ and $\langle \mathbf{F}(0) \rangle$ is proportional to the essential part of the alignment tensor; the trace $\mathrm{Tr}\langle \mathbf{F}(0) \rangle$ measures the average of squared bond lengths. For the maximum contour distance $d = N - 2$, we have $\mathbf{F}(N-2) = \sum_{i,j=1}^{N-1} \mathbf{u}_i \mathbf{u}_j$, the average of which is equal to the end-to-end tensor, and the trace $\mathrm{Tr}\langle \mathbf{F}(N-2) \rangle$ is equal to R_e, as given above. The uniaxial component $\Delta n(d)$ of $\mathbf{F}$, therefore, is a measure of the alignment in flow direction arising at a contour length d. Figure 8b shows that with increasing d the relaxation time of intramolecular alignment increases and that there is no pronounced behavior for specific contour lengths which could be only expected in case of the existence of schemes of typical arrangments at characteristic local length scales. The difference in local and global alignment becomes obvious in comparing the

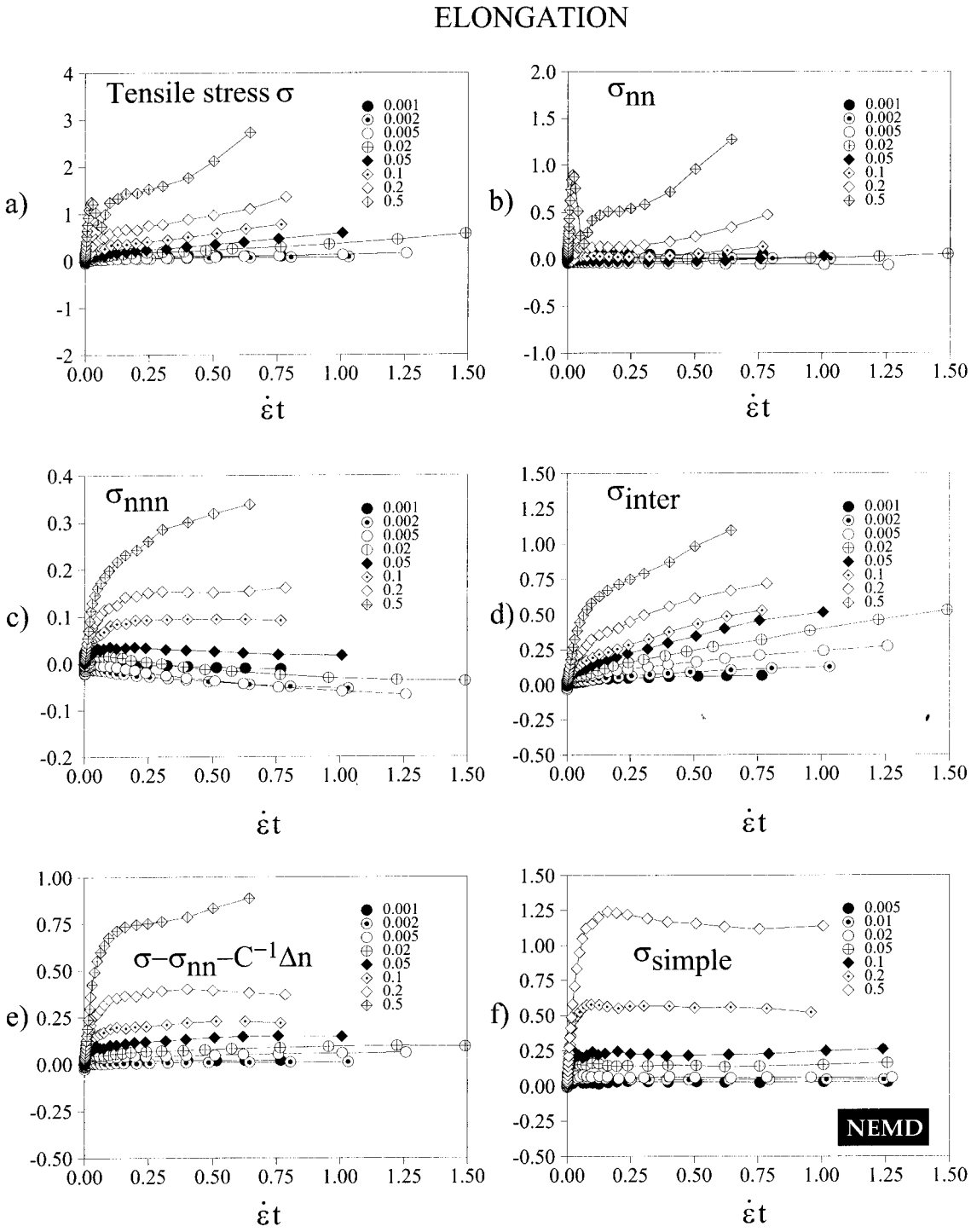

Figure 5. NEMD data for the tensile stress and its contributions arising at different initial elongation rates vs the dimensionless time $\dot{\epsilon}t$. The model polymer melt is composed of chains of length $N = 30$: (a) total stress σ, intramolecular contributions to σ from (b) nearest neighbors σ_{nn} and (c) non-nearest neighbors σ_{nnn}, (d) intermolecular contribution σ_{int}, (e) the polymeric stress $\sigma_{off} \equiv \sigma - \sigma_{nn} - C^{-1}\Delta n$ can be well compared with (f) the total stress σ_{simple} for the corresponding simple fluid ($N = 1$).

data for the uniaxial components ΔR_g of the gyration tensor and the flow alignment of segments $\Delta n \equiv \Delta n(1)$, as shown in Figure 7. At high rates the polymer coils deform affinely up to $\dot{\epsilon}t \approx 10$, while at fixed elongation the degree of segmental orientation decreases with decreasing rate, reflecting the fast orientational relaxation of segments compared with that of coils.

Stress−Optic Behavior. In Figure 9a the stress-alignment diagram is given, based on the data shown in Figures 5a, 6a, and Figure 7 (top). The results can be well compared with the experimental data as plotted in Figure 1b, c. Our results show (see Table 1, Figures 5, 6, and 9) that the stress tensor σ for the model polymer melts can be written essentially as the sum of three parts

$$\sigma \approx \sigma_{nn} + C^{-1}\Delta n + \tilde{\sigma}_{simple} \tag{8}$$

where σ_{nn} denotes the stress contribution from nearest neighbors within polymer chains (bond pushing/stretching or bond orientation or both) and σ_{simple} is proportional to the stress σ_{simple}, which is measured for a corresponding simple fluid by cutting all bonds within the system. A discussion of expression 8 is given in the next subsection.

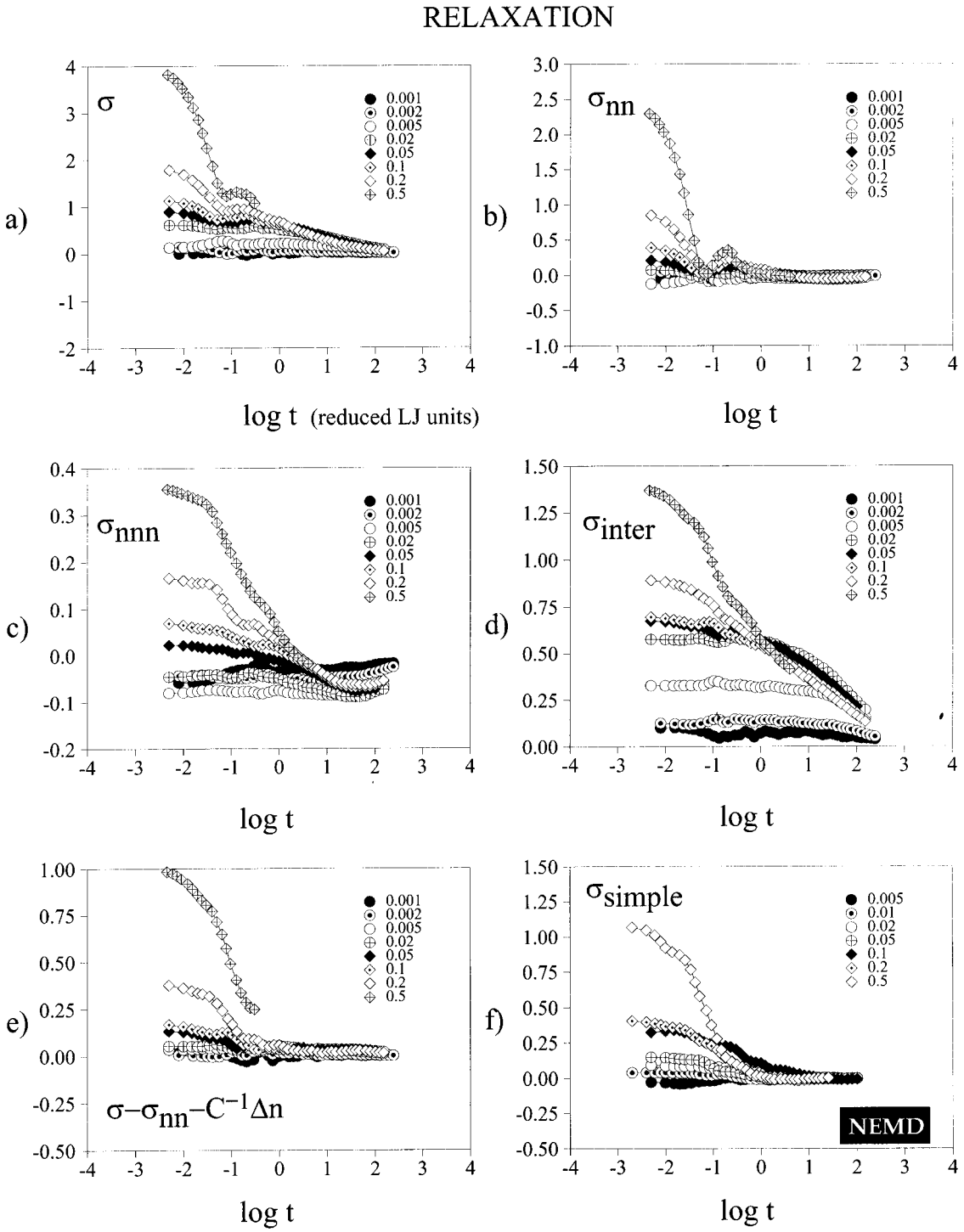

Figure 6. NEMD data for relaxation of the samples, elongation data of which are given in Figure 5.

It is a surprising result of the present investigation that the intermolecular stress σ_{int} has always a contribution proportional to the alignment of segments *and* that σ_{int} is dominating the total stress in two stages of the elongation−relaxation process. The intermolecular stress hence originates that part of the total stress ($C^{-1}\Delta n$ in eq 8) which yields the SOR at low rates or high temperatures where the remaining parts in eq 8 are small (see also Figure 10). From this follows that for the interpretation of the validity of the SOR the same argument could be used as for describing polymer melts by means of one-particle (single-link) theories: the polymer chains confined in the melt are ideal, i.e. they can be described without accounting for specific intermolecular local arrangements, the intermolecular pair correlation (IPCF) function should be similar to the one for the beads of a corresponding simple fluid, if the effect of preferable (anisotropic) orientation of links is properly removed from it. For oriented polymer melts, there is a stress contribution of every single link (or segment = two neighboring beads within a polymer chain) for purely geometrical reasons because the excluded volume of the links produce a directional screening of intermolecular interactions which is characterized directly by the alignment tensor. From this picture the IPCF for the polymer melt is then similar to the IPCF for the simple fluid corrected by a (scalar) term mainly linear in the alignment tensor. In sharp contrast to a set of previous approaches motivating the SOR by intramolecular forces,[23,38] the intermolecular contribution to the

Table 2. NEMD Data for Elongation−Relaxation with Rate $\dot{\epsilon} = 0.20$ and $N = 30$[a]

$t\dot{\epsilon}$ ($\dot{\epsilon} = 0.2$)	σ	σ_{nn}	σ_{nnn}	σ_{int}	Δn	σ_{simple}	σ_{off}
0.0002	0.01784	0.01544	0.00035	0.00254	0.00006	0.0065	0.0027
0.0004	0.03619	0.03084	0.00072	0.00509	0.00012	0.0129	0.0054
0.0009	0.08017	0.06891	0.00169	0.01154	0.00027	0.0290	0.0124
0.0016	0.14008	0.12060	0.00320	0.02083	0.00049	0.0515	0.0225
0.0025	0.21453	0.18182	0.00571	0.03304	0.00076	0.0767	0.0363
0.0045	0.34606	0.28238	0.01248	0.06151	0.00140	0.1311	0.0696
0.0073	0.42602	0.31734	0.02192	0.09398	0.00223	0.1930	0.1089
0.0122	0.39825	0.24089	0.03700	0.12439	0.00383	0.2912	0.1495
0.0200	0.23534	0.03628	0.05486	0.15013	0.00677	0.4129	0.1839
0.0300	0.32408	0.04492	0.07543	0.19977	0.01028	0.5020	0.2433
0.0500	0.42788	0.11356	0.09155	0.21897	0.01645	0.5237	0.2595
0.0782	0.50144	0.11112	0.11515	0.27846	0.02586	0.5797	0.3134
0.1271	0.62091	0.14172	0.11346	0.35598	0.04011	0.5756	0.3450
0.2034	0.65371	0.12063	0.14077	0.39187	0.05910	0.5346	0.3494
0.3029	0.77241	0.14037	0.15608	0.48597	0.08215	0.5670	0.3873
0.5029	0.96623	0.22692	0.15072	0.61504	0.11916	0.5451	0.3963
0.7857	1.35840	0.52158	0.16343	0.73502	0.17207	0.5558	0.3650
t ($\dot{\epsilon} = 0$)	σ	σ_{nn}	σ_{nnn}	σ_{int}	Δn	σ_{simple}	σ_{off}
0.010	1.691	0.764	0.161	0.882	0.21981	0.366	0.362
0.020	1.458	0.540	0.151	0.862	0.21967	0.356	0.333
0.035	1.220	0.287	0.162	0.847	0.21942	0.327	0.329
0.065	0.893	0.034	0.131	0.790	0.21841	0.234	0.244
0.105	0.930	0.135	0.084	0.754	0.21580	0.221	0.169
0.180	0.949	0.245	0.062	0.666	0.21015	0.138	0.077
0.300	0.862	0.167	0.070	0.646	0.20338	0.121	0.086
0.455	0.787	0.125	0.046	0.617	0.19498	0.046	0.059
0.775	0.681	0.072	0.030	0.590	0.18022	0.031	0.062
1.225	0.656	0.085	0.033	0.537	0.16699	0.008	0.052
2.000	0.531	0.029	0.009	0.492	0.15269	0.001	0.028
3.205	0.441	−0.005	−0.012	0.452	0.13639		0.017
4.775	0.388	−0.022	−0.022	0.433	0.12167		0.034
7.935	0.291	−0.040	−0.039	0.371	0.10255		0.013
12.41	0.249	−0.049	−0.050	0.348	0.08647		0.029
20.15	0.192	−0.055	−0.059	0.307	0.07204		0.024
47.95	0.120	−0.045	−0.064	0.228	0.04317		0.030
79.57	0.083	−0.034	−0.064	0.182	0.03063		0.023
102.0	0.074	−0.030	−0.059	0.163	0.02664		0.021
151.7	0.052	−0.025	−0.051	0.129	0.01989		0.016

[a] The measured stress σ is (by definition) the sum of the microscopic contributions σ_{nn},σ_{nnn},σ_{int},σ_{kin} (section III). One row includes the flow alignment Δn, the last two rows show the stress of a corresponding simple fluid σ_{simple} and the quantity σ_{off} (with $C = 3.1$)[3] contributing to the stress of the polymer fluid which is mainly responsible for the detected stress offset. There are significant similarities compared with σ_{simple} as discussed in the text (see also Figure 5). The polymer melt parameters are chain length $N = 30$, temperature $T = 1$, density = 0.84.

stress tensor (directly related to the IPCF) should hence be proportional to the alignment tensor if the single-link description is sufficient and if the corresponding viscous simple fluid (by cutting all bonds) is highly isotropic compared with the orientational flow-induced anisotropy of polymer segments.

Discussion of the Stress Tensor Expression. In contrast to the expressions of Read[20] or Gao and Weiner,[4] which were shortly reviewed in the Introduction, the three contributions in eq 8 have, by definition, precise microscopically meaning, as far as the FENE chain model is regarded as a microscopic model. To recall a phenomenological picture as reviewed in the introduction, the contributions σ_{nn} and $C^{-1}\Delta n$ are not equivalent to the contributions σ_d and σ_{or}, respectively, at least because σ_{nn} does not vanish at large deformations. On the basis of the assumption that the distortional part is dominant at short time scales, opposite to the orientational part made responsible for the long time behavior, both stresses (or moduli) are extracted easily if the limiting values C_d, C_{or} of the stress-optic coefficient (see section I) are known, via $\sigma_{or} = \sigma(t)(C(t) - C_d)/(C_{or} - C_d)$ and $\sigma_d = \sigma(t)(C_{or} - C(t))/(C_{or} - C_d)$, respectively. We find relationship (8) in good agreement with our simulations results (see Tables 2 and 3). The processes originating the term σ_{simple} do not directly affect the birefringence and can be identified with the source of the "stress offset".

In the following, the approximation (8) is motivated: For very low temperatures under elongation, i.e. for $T \rightarrow 0$, the stress for the isotropic and equilibrated model fluid is exactly the sum of the stresses which would arise for the corresponding LJ simple fluid (by cutting the bonds only) plus the contribution which stems from the intramolecular attractive FENE potential. The fluctuation-free ("perfect") affine motion of beads is independent of the information about neighboring bonds; from the homogeneous isochoric simulation of elongational flow, the affine motion is calculated for $T = 0$. The orientational relaxation times for connecting vectors between pairs of beads (during elongation at finite temperatures) are different for bonded and nonbonded pairs. The bonded pairs (neighbors within chains) have quite comparatively large relaxation times and depend on temperature. Since the stress σ_{nn} is the sum of the FENE part plus the LJ part of bonded neighbors at low temperatures, one gets directly $\sigma - \sigma_{nn} \equiv \sigma_{simple}$ with a proportionality factor which mainly depends on the lengths of chains, e.g. for $N = 1$ it is unity, for $N \rightarrow \infty$ it is constant and less than unity. At temperatures far above T_g and at small shear and elongation rates or large times during relaxation, the SOR is valid, in agreement with both a number of different theoretical arguments and experiments. Equation 8 hence can be regarded as the simplest type of a linear superposition of the two limiting cases. From this view our motivation

Table 3. NEMD Results for Elongation−Relaxation of Polymer Melts ($N = 30$) with $\dot{\epsilon} = 0.05$ (compare with Table 2)

$t\dot{\epsilon}$ ($\dot{\epsilon} = 0.05$)	σ	σ_{nn}	σ_{nnn}	σ_{int}	Δn	σ_{simple}	σ_{off}
0.00050	0.0347	0.0249	0.0025	0.0059	0.00015	0.014	0.008
0.00100	0.0560	0.0374	0.0068	0.0090	0.00031	0.032	0.015
0.00225	0.0522	0.0149	0.0176	0.0187	0.0008	0.066	0.034
0.00400	0.0237	−0.0264	0.0145	0.0348	0.0015	0.079	0.044
0.00625	0.0801	0.0119	0.0109	0.0526	0.0023	0.088	0.056
0.01150	0.0444	−0.0197	0.0170	0.0477	0.0041	0.103	0.052
0.01850	0.1170	0.0077	0.0241	0.0778	0.0061	0.121	0.083
0.03075	0.1014	−0.0086	0.0194	0.0908	0.0095	0.106	0.080
0.05000	0.1359	−0.0070	0.0394	0.1061	0.0149	0.132	0.099
0.07500	0.1172	−0.0180	0.0296	0.1050	0.0200	0.138	0.072
0.12500	0.1656	−0.0205	0.0313	0.1573	0.0286	0.130	0.099
0.19550	0.2166	−0.0220	0.0366	0.2011	0.0383	0.128	0.118
0.31775	0.2578	−0.0254	0.0300	0.2547	0.0520	0.128	0.123
0.50850	0.3491	−0.0214	0.0261	0.3451	0.0742	0.137	0.141
0.75725	0.4692	−0.0027	0.0184	0.4571	0.1042	0.132	0.152
t ($\dot{\epsilon} = 0$)	σ	σ_{nn}	σ_{nnn}	σ_{int}	Δn	σ_{simple}	σ_{off}
0.010	0.8657	0.1870	0.0225	0.6716	0.1817	0.128	0.130
0.020	0.7989	0.1284	0.0201	0.6617	0.1816	0.119	0.118
0.035	0.7103	0.0627	0.0142	0.6423	0.1814	0.110	0.094
0.065	0.6803	0.0341	0.0152	0.6427	0.1807	0.125	0.097
0.105	0.6707	0.0621	0.0060	0.6064	0.1795	0.074	0.055
0.180	0.7350	0.1472	0.0063	0.5878	0.1775	0.049	0.043
0.300	0.7377	0.1181	0.0101	0.6149	0.1760	0.067	0.079
0.455	0.6288	0.0494	−0.0052	0.5853	0.1740	0.023	0.040
0.775	0.6479	0.0682	−0.0098	0.5885	0.1687	0.017	0.055
1.225	0.5877	0.0332	−0.0117	0.5630	0.1630	0.006	0.045
2.000	0.5440	0.0280	−0.0223	0.5401	0.1558	0.001	0.034
3.205	0.5043	0.0091	−0.0262	0.5235	0.1444		0.049
4.775	0.4320	−0.0134	−0.0354	0.4822	0.1334		0.033
7.935	0.3699	−0.0315	−0.0478	0.4492	0.1182		0.034
12.40	0.3009	−0.0525	−0.0609	0.4133	0.1032		0.032
20.15	0.2523	−0.0596	−0.0682	0.3802	0.0881		0.038
32.21	0.1946	−0.0635	−0.0751	0.3315	0.0711		0.035
63.75	0.1366	−0.0536	−0.0744	0.2648	0.0503		0.034
101.93	0.0910	−0.0434	−0.0717	0.2063	0.0347		

is on the same qualitative level as the superposition of orientational and distortional stresses as proposed earlier. As determined by NEMD the kinetic part of the stress tensor plays no role for polymer melts up to the stretching ratios studied here.

Stretching on Different Length Scales. To resolve between stretching and orientation on different length scales which cannot be done by investigating the anisotropic components of the alignment tensor and gyration tensor alone, we plot in Figure 8a the time dependence of the (normalized) spatial distance $\Delta r(d) \equiv \mathrm{Tr}\langle \mathbf{F}(d)\rangle / \mathrm{Tr}\langle \mathbf{F}_{eq}(d)\rangle$ between points with given contour distance d along the polymers backbone. Notice that $\Delta r(0)$ is a scalar measure for the deviation of the distribution of (squared) bond lengths from its equilibrium distribution. The change of the shape of this distribution under nonequilibrium conditions as plotted in Figure 11 provides more information than $\Delta r(0)$. The deviations indirectly imply deviations from a proportionality between alignment of segments and the stress σ_{nn} (arising from segments) which result in the pronounced increase of stress, especially at the early and the late stage of elongation. Under relaxation, σ_{nn} approximately vanishes while deviations from the equilibrium distribution are being present.

The bond length autocorrelation function $\langle G(d)\rangle$ as defined in eq 7 is plotted in Figure 12. It measures collective stretching of neighboring bonds which are separated by d segments. Since $\langle G(0)\rangle = \sum_{i=1}^{N-1} \langle (u_i - \bar{u})^2\rangle/(N-1)$ is the width of the distribution of bond lengths, $\langle G(1)\rangle$ is a measure for the collective deformations of directly neighboring ($d = 1$) segments, and so on up to $d = N - 2$. With decreasing correlation for increasing distance d, the quantity $\langle G(d)\rangle$ "relaxes" to zero. Recently, experimental results of time-resolved optical spectroscopy[40] were inconsistent with some models of cooperative molecular motion near T_g which invoke rigid aggregates or locally liquidlike regions whereas localized stretching of chains has been evoked in studies on plastic deformation of glassy polymers.[41] No pronounced collective stretching is observed from the NEMD results at small elongations. This finding is in agreement with our results on dumbbell fluids for which the qualitative behavior is surprisingly similar while collective stretchings are impossible. The dumbbell results can be described too by relation (8).

The quantity defined in eq 7 was introduced to check if the failure of the stress−optical rule at high rates could be explained by considering that only a few single segments are strongly stretched (i.e. in the nonlinear part of the FENE force law), giving rise to an important contribution to the stress without influencing the mean alignment.

For this scheme no evidence is found by analyzing the NEMD results. Only at a late stage of elongation, when segmental stretching leads to a strong increase in σ_{nn}, are local inhomogeneities in bond stretchings/contractions found, whereby expression (8) remains valid.

Yield Point. There are various molecular pictures in the literature that are able to explain the origin of the stress overshoot (Figures 5 and 9). The most common ones deal with the occurrence of molecular processes of local strain production (inhomogeneous deformation)

On the basis of the information contained in Figures 7, 8, 11, and 12, our investigations lead to the following picture: At start up of elongation, all particles of the system, especially the bonds, perform a perfect affine

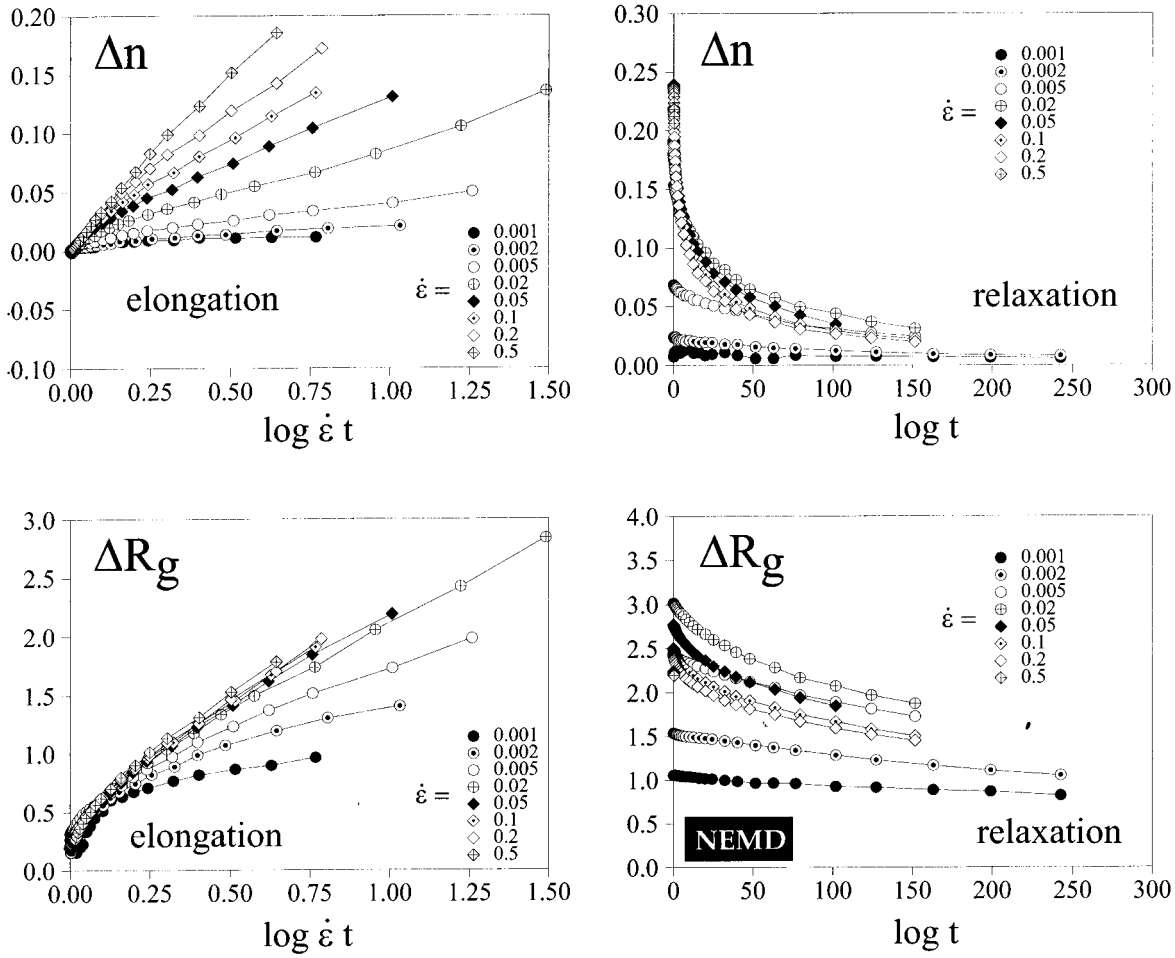

Figure 7. NEMD data for the same parameters as in Figures 5 and 6. (top) Flow alignment of segments Δn and (bottom) polymer coils ΔR_G for elongation−relaxation at different rates. The quantities are defined in section IV.

motion corresponding to the strong stress increase (proportional to the alignment but with a small stress-optic coefficient compared with the increase measured on the "equilibrium curve"; Figures 1 and 9) which depends only on the macroscopic elongation of the sample. The length of the time interval of affine motion is determined by the ratio of temperature/rate, density, and constraints which hinder orientational diffusion of segments.

Because of the constraints, the segmental relaxation time is large compared with the relaxation time for intermolecular correlations, and therefore, σ_{nn} is the leading term in this regime. Moreover, the main contribution to the affine stress stems from bonds which are perpendicular to the stretching direction because of the shape of the FENE + LJ potential. The period ends with the inset of orientational diffusion of segments (nonaffine motion) in the direction of macroscopic flow. At this time the initially stretched/contracted bonds remain to oscillate around their equilibrium values while dynamically correlated with its neighbors (see the gray shadows at intermediate times during elongation in Figure 12), and the contribution σ_{nn} becomes unimportant compared to the part of that intermolecular stress part which is fulfilling the SOR. As described above, this contribution can be regarded as geometric in nature. Upon increasing the stretching ratio, the response of the system to the external forces is not due to alignment of segments only, but deviations from the distribution of bond lengths from its equilibrium state lead to an increase of importance of the σ_{nn} part which is nonlinear in the alignment Δn. For high elongation

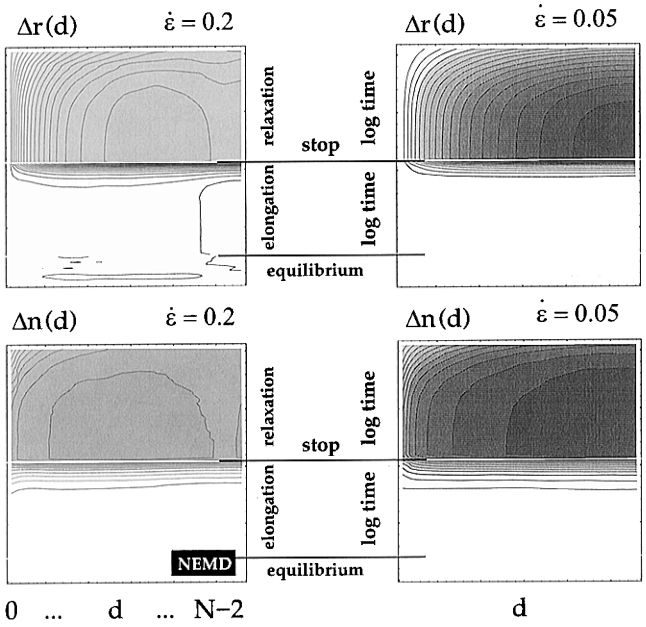

Figure 8. NEMD data to analyze the degree of stretching (distance Δr) and orientation (Δn) of the polymer chains on different length scales d, where d is the distance between two beads of the same chain measured along the chains contour. More precisely, by use of eq 6 we can write $\Delta r(d) \equiv \mathrm{Tr}\langle \mathbf{F}(d)\rangle / \mathrm{Tr}\langle \mathbf{F}_{eq}(d)\rangle$ and $\Delta n(d) \equiv \langle F_{xx} - (F_{yy} - F_{zz})/2\rangle$. These quantities are sensitive to the changes compared with the equilibrium values; they are of use in measuring intramolecular inhomogeneities in stretching and alignment. The plotted range is (from white to black) [0,6] for $\Delta r(d)$ and [0,3] for $\Delta n(d)$.

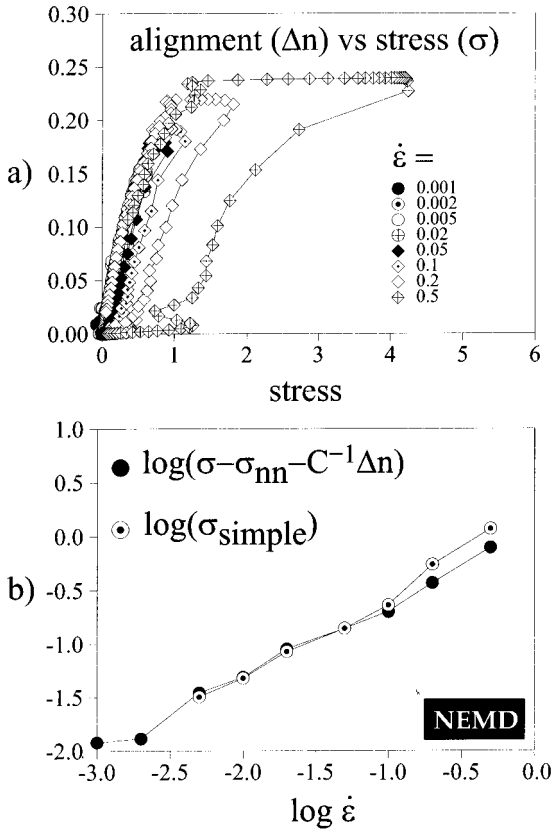

Figure 9. NEMD data. (a) Stress-alignment diagram for the same parameters as in Figure 5. (b) Double logarithmic plot of the stress offset (as defined by $\sigma_{off} \equiv \sigma C^{-1}\Delta n - \sigma_{nn}$) with $C^{-1} = 3.1$[3] and the stress of the simple fluid (σ_{simple}) vs elongation rate. The values for each rate $\dot{\epsilon}$ were extracted in time intervals of approximatively time-independent offset (see also Tables 2 and 3).

rates or low temperatures, therefore, a yield point can be interpreted without referring to spatial inhomogeneities as long as not all local perturbations from affine motion are considered as spatial inhomogeneities.

Even in nonisochoric simulations (NPT ensemble) a yield point in the load is obtained, e.g. for $N = 120$, T = 1, $\dot{\epsilon} = 0.1$.[42] For comparison with the results shown for polymer chains, NVT simulations for elongation−relaxation of dumbbells ($N = 2$) at rates $\dot{\epsilon} = 0.05$ and 0.2 have been performed. As for the long chains, a slight stress overshoot is detected which becomes more pronounced at higher rates. Again, the expression for the stress tensor (8) is valid while intramolecular correlations or non-nearest neighbor interactions are nonexistent. The orientational relaxation time is shorter than for the polymers with $N = 30$ beads, resulting in a shift of the yield point (occurring for $\dot{\epsilon} = 0.2$) to short times. As before, the stress contribution fulfilling the SOR stems from intermolecular interactions alone.

VI. Summary and Conclusions

The multibead spring model for a polymer melt was implemented in a nonequilibrium molecular dynamics simulation of an isochoric uniaxial elongational flow. The model systems qualitatively resemble the behavior found for real polymer melts for which results are presented here. Data were presented for four decades in the rate, beginning with a regime of valid SOR for the lowest rates. The model systems exhibited deviations from the SOR and a yield point at high rates. Within the simulations, the rheological quantities and all its microscopic contributions are simultaneously accessible together with quantities measuring the anisotropy of the system. Emphasis was laid on the underlying microstructural changes, i.e., a flow-induced alignment on local and global lengths scales or collective stretching of bonds, and on the microscopic contributions to the measured stress.

The main conclusions from this investigation can be summarized as follows.

(i) Stress-Optic Rule. The proportionality between stress and alignment tensor is verified for small elongation rates or high temperatures. However, violations as reflected by the occurrence of a "stress offset" are observed for higher rates and temperatures close to T_g.

(ii) Distortion of the Polymer Coil. The strength of alignment increases with the intramolecular length scale at any fixed time as shown by investigating the alignment of segments, the radius of gyration, the end-to-end distance, and all intermediate length scales by the quantity $F(d)$ (Figures 7 and 8). These results give an impression of the shape of the static structure factors (measurable by SANS and directly from the computer simulation)[3] in the reciprocal space (of wave vector transfer).

(iii) Scaling Behavior of the Stress Offset. A rate-dependent contribution to the stress which is not directly related to the intramolecular conformations

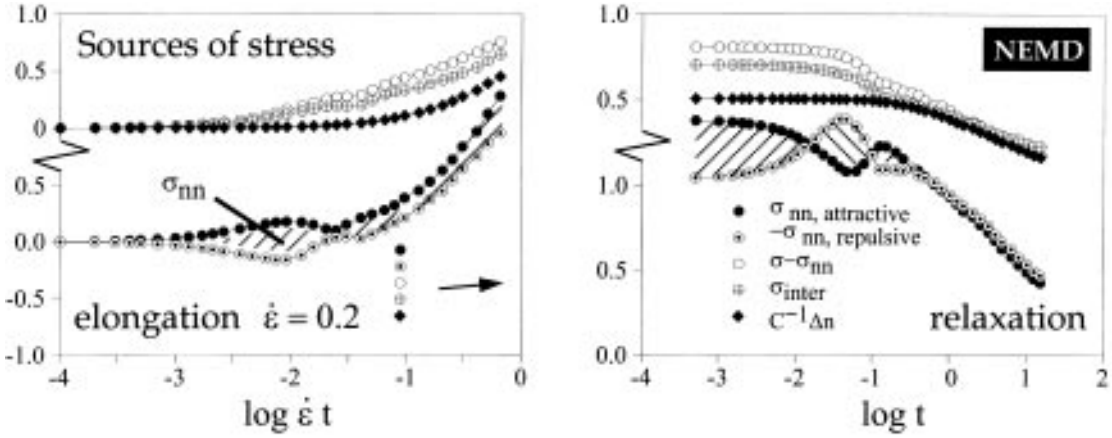

Figure 10. NEMD data. Contributions to the total deviatoric stress σ from nearest neighbors within chains (σ_{nn}) (its repulsive and attractive part is shown, too) and from intermolecular interactions between different chains (σ_{int}). The stress obeying the SOR is included as $C^{-1}\Delta n$, where $C = 3.1$ is determined from the high temperature behavior and independently from computer simulation on weak shear flow.[3]

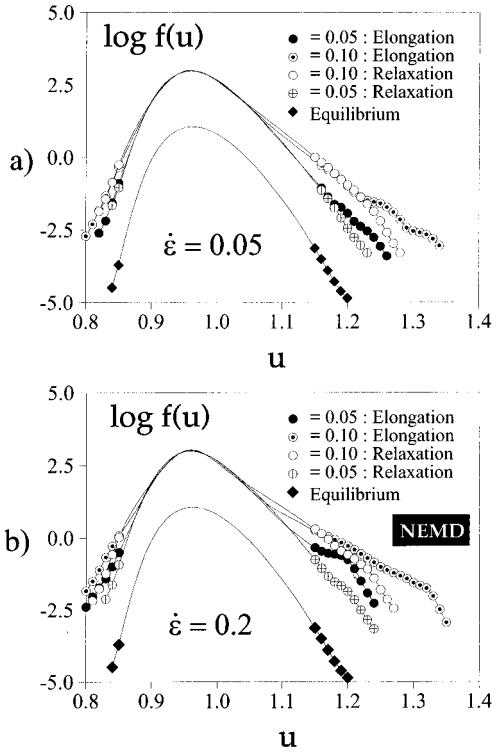

Figure 11. NEMD data. Distribution $f(u)$ of bond lengths u for the elongation rates $\dot{\epsilon} = 0.05$ and 0.2 at three different times in both elongation and relaxation with equal values of the degree of alignment (cf. Figure 7) is plotted together with the corresponding Boltzmann distribution ("equilibrium") calculated simply by the intramolecular model potential (Figure 3).

("stress offset") is detected in both experiment and simulation. In a wide range of elongation rates, a linear dependence of the stress offset on rate is found.

(iv) Collective Stretching of Bonds. Stretching is not pronounced in the vicinity of the yield point but gets important at high deformations.

(v) Yield Point: The Concurrent Mechanisms. Affine motion and reorientational diffusion of segments determine the (non)occurrence of the stress overshoot. The relevance of both mechanisms on different time scales is strongly influenced by the system parameters, temperature, density, rate, and model potentials.

(vi) Relaxation of Elongated Polymer Melts. The relaxation behavior of elongated samples in both experiment and simulation is found to be independent of the initial rate. In the stress−optical diagram the curves fall on the "equilibrium curve" which finally obeys the SOR. Most surprisingly, intermolecular interactions alone are shown to be responsible for the validity of the SOR.

(vii) Spatial Inhomogeneities and Influence of the Molecular Weight. From the NVT computer simulations, no evidence is found for the qualitative stress−optical behavior being dominated by spatial inhomogeneities in both density or alignment. Even if the molecular weight of both sets of presented data are not comparable, they do not discuss different regimes in view of the physical mechanisms involved in the discussion of the rheological effects under study. Runs performed by us on model polymer melts with $N = 300$ which is well above the entanglement length confirmed this picture.

(viii) Approximate Expression for the Stress Tensor. In agreement with the computer simulation

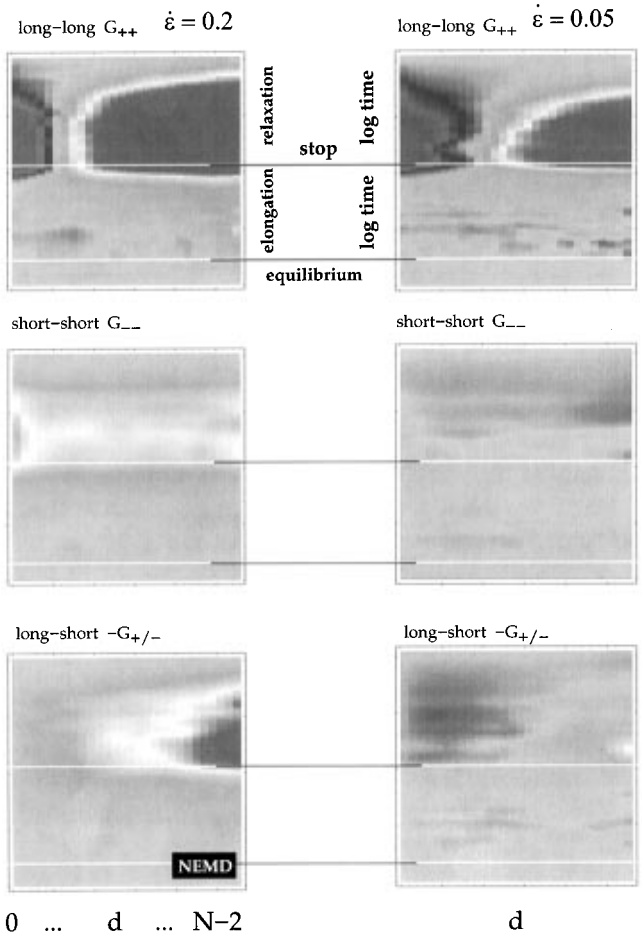

Figure 12. NEMD data. Contributions to the (discrete) bond length autocorrelation function as defined in eq 7. The different contributions G_{++}, G_{--}, and $-G_{\pm}$ are functions of the contour distance d and resolve collective stretching, contraction, and compensations of bonds, especially those which are far from their equilibrium values. Shown are the deviations of the quantities from their equilibrium functions. The plotted range is (from white to black) [−6,6].

results, we propose an expression for the stress tensor for polymer melts which is related to the flow-induced alignment (Δn) and stretching/contraction of bonds (σ_{nn}) and to the stress arising for a corresponding simple fluid (σ_{simple}) at the same bead number density and temperature. The latter is responsible for the nearly time-independent viscosity offset which becomes important at high rates or low temperatures because in these regimes the viscosity of the simple fluid is comparable to the viscosity of a polymer liquid (as is the case at high shear rates too).

A relevant feature of our expression (8) is that, starting from a mesoscopic theory, e.g. a Fokker−Planck equation for the configurational distribution function (CDF) of multibead (flexible) polymer chains,[5,23,38,43,44] one can compute directly both the birefringence Δn and the stress σ_{nn}. Together with the theoretical results for the stresses arising for the corresponding simple fluid,[45] the total stress can be computed, which is not the case for the stress tensor expressions proposed earlier for polymers near T_g,[4,20] because the stresses σ_d and σ_{or} are not separately well-defined. Notice that also the deviations from the SOR for the same model polymer melts under shear flow[3,5] can be interpreted by the three-part expression; the characteristic shear rate at the onset of deviations was detected to be independent of the chain length N.[3] This is consistent with including the term

proportional to σ_{simple} into the formulation (8) which represents a term quite independent of N.

Structural anisotropies accompanying the viscoelastic behavior will be presented in a subsequent paper; it will allow for a test of further correspondence between both experiment and theory.

Acknowledgment. The author M.K. thanks the Sonderforschungsbereich 335 "Anisotrope Fluide" and the Graduiertenkolleg "Polymerwerkstoffe" (Berlin) of the Deutsche Forschungsgemeinschaft for financial support, as well as the Konrad-Zuse-Zentrum für Informations-technik (Berlin) and the German supercomputing center (HLRZ) of the Kfa Jülich GmbH for their generous donation of CPU time on CRAY Y-MP 4D/464 and CRAY J916/16−4096 vector machines. Enlighting discussions with H. C. Öttinger, G. Marrucci, R. G. Larson, S. Hess, and C. Picot are gratefully acknowledged.

References and Notes

(1) Kremer, K.; Grest, G. S. *J. Chem. Phys.* **1990**, *92*, 5057.
(2) Lopez Cascales, J. J.; Navarro, S.; Delatorre, J. G. *Macromolecules* **1992**, *25*, 3574.
(3) Kröger, M.; Loose, W.; Hess, S. *J. Rheol.* **1993**, *37*, 1057.
(4) Gao, J.; Weiner, J. H. *J. Chem. Phys.* **1992**, *97*, 8698; *Macromolecules* **1994**, *27*, 1201; **1996**, *29*, 6048.
(5) Kröger, M. *Rheologie und Struktur von Polymerschmelzen*; Wissenschaft & Technik Verlag: Berlin, 1995.
(6) Hounkonnou, M. N.; Pierleoni, C.; Ryckaert, J.-P. *J. Chem. Phys.* **1992**, *97*, 9335.
(7) Fetsko, S. W.; Cummings, P. T. *J. Rheol.* **1995**, *39*, 285.
(8) Kobe, J. M.; Wiest, J. M. *J. Rheol.* **1993**, *37*, 947.
(9) Kröger, M.; Makhloufi, R. *Phys. Rev. E* **1996**, *53*, 2531.
(10) Kröger, M. *Rheology* **1995**, *5*, 66.
(11) Kröger, M.; Voigt, H. *Macromol. Theory Simul.* **1994**, *3*, 639.
(12) Laun, H. M.; Bung, R.; Hess, S.; Loose, W.; Hess, O.; Hahn, K.; Hädicke, E., Hingmann, R.; Schmidt, F.; Lindner, P. *J. Rheology* **1992**, *36*, 743.
(13) Loose, W.; Hess, S. *Rheol. Acta* **1989**, *28*, 91.
(14) Kalus, J.; Hoffmann, H. *J. Chem. Phys.* **1987**, *87*, 714.
(15) Muller, R.; Picot, C. *Makromol. Chem.—Makromol. Symp.* **1992**, *56*, 107. Muller, R.; Pesce, J. J.; Picot, C. *Macromolecules* **1993**, *26*, 4356.
(16) Muller, R.; Pesce, J. J. *Polymer* **1994**, *35*, 734. The equilibrium curve represents the stress−optical behavior of the melt at temperatures high enough with respect to the T_g to be independent of both temperature and elongation rate, even in the nonlinear part at high stresses.
(17) Pick, M.; Lovell, R. *Polymer* **1979**, *20*, 1448.
(18) Janeschitz-Kriegl, H. J. *Polymer melt rheology and flow birefringence*; Springer: Berlin, 1983.
(19) Priss, L. S.; Vishnyakoov, I. I.; Pavlova, I. P. *Int. J. Polym. Mater* **1980**, *8*, 85.
(20) Read, B. E. *Polym. Eng. Sci.* **1983**, *23*, 835
(21) Osaki, K.; Okamoto, H.; Inoue, T.; Hwang, E.-J. *Macromolecules* **1995**, *28*, 3625, and refs 4 and 6 herein.
(22) Gao, J; Weiner, J. H. *J. Chem. Phys.* **1989**, *90*, 6749.
(23) Doi, M.; Edwards, S. F. *The theory of polymer dynamics*; Clarendon: Oxford, 1986.
(24) Mead, D. W.; Leal, L. G. *Rheol. Acta* **1995**, *34* 339. Mead, D. W.; Yavich, D.; Leal, L. G. *Rheol. Acta* **1995**, *34*, 360.
(25) Muller, R.; Froelich, D. *Polymer* **1985**, *26*, 1477.
(26) Inoue, T.; Okamoto, H.; Osaki, K. *Macromolecules* **1991**, *24*, 5670. Okamoto, H.; Inoue, T.; Osaki, K. *Macromolecules* **1992**, *25*, 3413.
(27) Tassin, J. F.; Monnerie, L. *Macromolecules* **1988**, *21*, 1846.
(28) Siesler, H. W.; Pfeifer, F.; Luap, C., unpublished results.
(29) Hess, S. *J. Non-Newt. Fluid Mech.* **1987**, *23*, 305.
(30) Feigl, K.; Öttinger, H. C. *J. Rheol.* **1994**, *38*, 847.
(31) de Gennes, P. G. *Scaling concepts in polymer physics*; Cornell Univ. Press: Ithaca, NY, 1979.
(32) Warner, H. R. *Ind. Eng. Chem. Fund.* **1972**, *11*, 379.
(33) Weeks, J. D.; Chandler, D.; Andersen, H. C. *J. Chem. Phys.* **1971**, *54*, 5237.
(34) Verlet, L. *Phys. Rev.* **1957**, *159*, 98.
(35) Rapaport, D. C. *Comput. Phys. Rep.* **1988**, *9*, 1; *Comput. Phys. Commun.* **1991**, *62*, 198.
(36) Allen, M. P.; Tildesley, D. J. *Computer simulation of liquids*; Clarendon: Oxford, 1987.
(37) Evans, D. J. *Mol. Phys.* **1979**, *37*, 1745. Evans, D. J.; Hoover, W. G.; Failor, B. H.; Moran, B.; Ladd, A. J. C. *Phys. Rev. A* **1983**, *28*, 1016.
(38) Bird, R. B.; Hassager, O.; Armstrong, R. C.; Curtiss, C. F. *Dynamics of polymeric liquids*; Wiley & Sons: NY, 1987; Vols. 1 and 2.
(39) Bowden, P. B. *The physics of glassy polymers*; Haward, R. N., Ed.; Wiley: New York, 1973.
(40) Cicerone, M. T.; Blackburn, F. R.; Ediger, M. D. *J. Chem. Phys.* **1995**, *102*, 471.
(41) Achibat, T.; Boukenter, A.; Duval, E.; Mermet, A.; Aboulfaraj, M.; Etienne, S.; G'Sell, C. *Polymer* **1995**, *36*, 251.
(42) Voigt, H. Struktur und Dynamik in Polymerschmelzen und -gläsern. Thesis; TU Berlin, 1996.
(43) Öttinger, H. C. *J. Non-Newtonian Fluid Mech.* **1987**, *26*, 207.
(44) Wedgewood, L. E.; Öttinger, H. C. *J. Non-Newtonian Fluid Mech.* **1988**, *27*, 245.
(45) Kim, J. J.; Jeong, S. H. *J. Phys. A* **1987**, *20*, 3631. Evans, D. J. *Physica A* **1983**, *118*, 51. Heyes, D. M. *J. Chem. Soc. Faraday Trans. 2* **1983**, *79*, 1741, and refs therein. Ryckaert, J.-P.; Bellemans, A. *Phys. Rev. Lett.* **1988**, *60*, 128.

MA960317C